Quantitative Susceptibility Mapping identifies hippocampal and other subcortical gray matter tissue composition changes in temporal lobe epilepsy

Oliver C. Kiersnowski[1], Gavin P. Winston[2,3], Lorenzo Caciagli[2,4], Emma Biondetti[1,5], Maha Elbadri[6], Sarah Buck[2], John S. Duncan[2], John S. Thornton[7], Karin Shmueli[1†], Sjoerd B. Vos[7,8,9†]

[†]**These authors contributed equally to this work.**

Author affiliations:

1 Department of Medical Physics and Biomedical Engineering, University College London, London, United Kingdom

2 Department of Clinical and Experimental Epilepsy, University College London, London, United Kingdom

3 Department of Medicine, Division of Neurology, Queen's University, Kingston, Canada

4 Department of Bioengineering, University of Pennsylvania, 240 South 33rd Street, Philadelphia, Pennsylvania, U.S.A.

5 Department of Neuroscience, Imaging and Clinical Sciences, Institute for Advanced Biomedical Technologies, "D'Annunzio" University of Chieti-Pescara, Chieti, Italy

6 Department of Neurology, Queen Elizabeth Hospital, Birmingham, United Kingdom

7 Neuroradiological Academic Unit, UCL Queen Square Institute of Neurology, University College London, London, United Kingdom

8 Centre for Microscopy, Characterisation, and Analysis, The University of Western Australia, Nedlands, Australia

9 Centre for Medical Image Computing, Computer Science department, University College London, London, United Kingdom

Corresponding author: Oliver C. Kiersnowski
Malet Place Engineering Building, Department of Medical Physics & Biomedical Engineering, University College London, London, WC1E 7JE
o.kiersnowski@ucl.ac.uk

Running title (40 chars): QSM identifies tissue changes in TLE

Abstract

Temporal lobe epilepsy (TLE) is associated with widespread brain alterations. Using quantitative susceptibility mapping (QSM) alongside transverse relaxation rate (R_2^*), we investigated regional brain susceptibility changes in 36 patients with left-sided (LTLE) or right-sided TLE (RTLE) secondary to hippocampal sclerosis, and 27 healthy controls (HC). We compared three susceptibility calculation methods to ensure image quality. Correlations of susceptibility and R_2^* with age of epilepsy onset, frequency of focal-to-bilateral tonic-clonic seizures (FBTCS), and neuropsychological test scores were examined. Weak-harmonic QSM (WH-QSM) successfully reduced noise and removed residual background field artefacts. Significant susceptibility increases were identified in the left putamen in the RTLE group compared to the LTLE group, the right putamen and right thalamus in the RTLE group compared to HC, and a significant susceptibility decrease in the left hippocampus in LTLE vs HC. LTLE patients who underwent epilepsy surgery showed significantly lower left-vs-right hippocampal susceptibility. Significant R_2^* changes were found between TLE and HC groups in the amygdala, putamen, thalamus and in the hippocampus. Specifically, decreased R2* was found in the left and right hippocampus in LTLE and RTLE, respectively, compared to HC. Susceptibility and R_2^* were significantly correlated with cognitive test scores in the hippocampus, globus pallidus, and thalamus. FBTCS frequency correlated positively with ipsilateral thalamic and contralateral putamen susceptibility and with R_2^* in bilateral globi pallidi. Age of onset was correlated with susceptibility in the hippocampus and putamen, and with R_2^* in the caudate. Susceptibility and R_2^* changes observed in TLE groups suggest selective loss of low-myelinated neurons alongside iron redistribution in the hippocampi, predominantly ipsilaterally, indicating QSM's sensitivity to local pathology. Increased susceptibility and R_2^* in the thalamus and putamen suggest increased iron content and reflect disease severity.

Keywords: quantitative susceptibility mapping; temporal lobe epilepsy; hippocampal sclerosis; refractory epilepsy; quantitative MRI

Abbreviations: BFR = background field removal; FAS = focal aware seizures; FBTCS = focal-to-bilateral tonic-clonic seizures; FIAS = Focal impaired aware seizures; GE = gradient echo; GP = globus pallidus; HC = healthy controls; HS = hippocampal sclerosis; LTLE = left temporal lobe epilepsy; QSM = quantitative susceptibility mapping; R_2^* = transverse relaxation rate; ROI = region of interest; RTLE = right temporal lobe epilepsy; TLE = temporal lobe epilepsy; TV = total variation; WH-QSM = weak harmonic quantitative susceptibility mapping;

Introduction

Temporal lobe epilepsy (TLE) is the most common type of focal epilepsy. Hippocampal sclerosis (HS) is the most common histopathological cause of TLE[1], and is characterized by atrophy and loss of internal tissue architecture on neuroimaging and, microscopically, by neuronal cell loss and gliosis[2]. Magnetic resonance imaging (MRI) is a key tool in the diagnosis of HS, with hippocampal atrophy and signal hyperintensities on T_2-weighted images seen in most patients[2]. Further improvements in diagnostic performance have been obtained from quantification of MRI abnormalities[3].

Although seizures in TLE arise focally from the temporal lobe, MRI has revealed changes at cortical and subcortical levels. A recent meta-analysis of cortical volumetry shows strong evidence for temporal and extratemporal cortical volume loss in TLE related to epilepsy disease duration[4], supported by a longitudinal study showing widespread cortical atrophy in TLE compared to age-matched controls[5]. Subcortically, there are bilateral thalamic volumetric changes in TLE that relate to disease duration[6], alterations in diffusivity properties throughout the white matter[7], and functional connectivity changes in the thalamus and basal ganglia[8,9]. Transverse relaxation rate (R_2^*) maps have been used to investigate the hippocampus in TLE with HS significantly associated with R_2^* reductions in the hippocampus of TLE patients compared to healthy controls but no significant R_2^* differences found between TLE patients with and without HS[10]. Quantitative MRI methods such as myelin mapping and neurite density imaging have only recently seen applications in TLE, revealing widespread cortical and subcortical changes[11]. Here, we explore the contributions of a different quantitative MRI technique, quantitative susceptibility mapping (QSM).

QSM[12–14] is a quantitative MRI technique that relies on images acquired from gradient-echo based sequences (commonly T_2^*-weighted images) and calculates the tissue magnetic susceptibility distribution, χ, from the phase component, ϕ, of the complex MRI signal. There are three key steps in the QSM pipeline: i) phase unwrapping, which removes the artificial phase wraps present in phase images due to ϕ being constrained to the $[-\pi, \pi)$ interval; ii) background field removal (BFR), which separates and removes the magnetic field perturbations due to external χ sources (such as the skull and air), leaving the local fields from the χ sources of interest inside the brain; iii) susceptibility calculation from the local fields through field-to-source or dipole inversion. This is an ill-posed problem solved using various mathematical regularisation strategies[15,16], each with different benefits for particular applications[17–19]. QSM has successfully identified subtle tissue composition changes, for example, in paediatric epilepsy to reveal susceptibility changes in focal cortical dysplasia lesions, consistent with reduced iron and myelin and increased calcium and zinc content[20]. QSM has also been used to successfully derive oxygen extraction fraction maps in epilepsy patients[21], and has been suggested as a possible biomarker for diagnosis and treatment monitoring in cerebral cavernous malformations[22], a common cause of epilepsy. Furthermore, QSM has been used to investigate changes in susceptibility in the presumed seizure-onset zone between postictal and interictal states in three subjects with TLE, where increased susceptibility was found postictally compared to interictally[23].

Here, we extend the application of QSM in epilepsy by investigating susceptibility changes in the hippocampus, amygdala, thalamus, and basal ganglia in people with TLE and unilateral HS. Further, we compared three susceptibility calculation methods with respect to the quality of their corresponding susceptibility maps, to ensure adequate noise and residual background field removal. We also included comparisons of R_2^*, because R_2^* and susceptibility provide complementary information regarding the underlying tissue composition changes. Finally, we correlated χ and R_2^* with clinical characteristics – including neuropsychology data, age of disease onset, and seizure type and frequency – to assess the potential sensitivity of these quantitative MRI measures to disease severity.

Materials and methods

Participants

We included a total of 41 participants with TLE and unilateral HS, who attended the Chalfont Centre for Epilepsy at Chalfont St Peter, Buckinghamshire, United Kingdom for routine examination. We also included 29 healthy controls. Visual inspection showed poor image quality due to artefacts (Supplementary Figure 1) in five TLE participants and two controls. Therefore, the final cohort consisted of 36 TLE participants and 27 healthy controls (see Table 1 for demographics). Nine patients underwent anterior temporal lobectomy. This project was approved by the London–Bloomsbury Research Ethics Committee (REC reference: 20/LO/0149) and comprised retrospective research conducted on clinically acquired data that did not pose risk to any patients. Written informed consent was obtained from each healthy control through studies approved by the National Hospital for Neurology and Neurosurgery and the UCL Institute of Neurology Joint Research Ethics Committee. For TLE participants, the following clinical characteristics were available: seizure type and frequency, disease duration, and age of epilepsy onset. For FBTCS[8,9], this was further specified depending on whether patients had FBTCS in the twelve months preceding the MRI scan (called the ‘recent’ group), only longer than twelve months ago (the ‘historic’ group), or never, as in Caciagli et al[9].

Data Acquisition and Processing

All subjects were imaged on a 3T General Electric Discovery MR750 scanner with a 32-channel head RF receive coil. Sequences included a T_1-weighted inversion recovery fast spoiled gradient-recalled echo (TE/TR/TI = 3.1/7.4/400 ms, field of view (FOV) $224 \times 256 \times 256$ mm, matrix size $224 \times 256 \times 256$, 1-mm isotropic voxel size, parallel imaging factor = 2; acquisition time 4 min 19 s). Subjects also underwent a multi-echo 3D gradient-echo (SWAN) sequence, acquired with oblique axial acquisition along the AC-PC line, with monopolar readout gradients, in which the complex (magnitude and phase) images were saved (TE1/ΔTE/TE5 = 12.9/5.0/32.8 ms, TR = 37.1 ms, flip angle = 15°, FOV $200 \times 200 \times 137$ mm, matrix size $384 \times 384 \times 114$, reconstructed to a voxel size of $0.52 \times 0.52 \times 0.60$ mm through zero-padding by a factor of 2 in the last dimension; acquisition time 6 min 30 s).

Regions of interest (ROIs) in the amygdala, caudate nucleus, globus pallidus (GP), putamen, and thalamus were segmented on the 3D T_1-weighted images using GIF[24–26]. To ensure accurate hippocampal segmentation in the presence of hippocampal pathology, HippoSeg[27] was used to segment the hippocampus. The T_1-weighted images were rigidly registered to the first-echo magnitude image of the QSM SWAN data using NiftyReg[28]. The resulting transformation was then used to align the ROIs with the SWAN data (Figure 1).

R_2^* maps were calculated via a least-squares linear fit of the logarithm of the magnitude images over echo times using the FANSI toolbox[29].

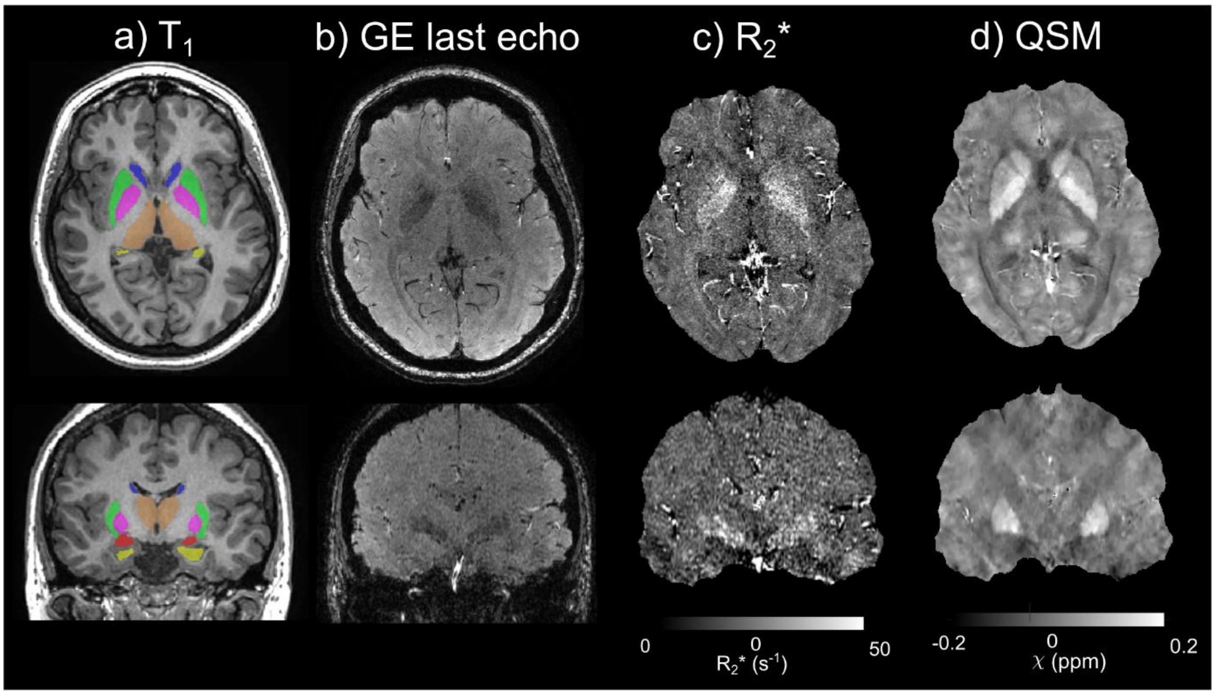

Figure 1: Images from a representative subject: T_1-weighted image, gradient echo magnitude image, R2* map and Susceptibility map. a) T_1-weighted image with ROIs superimposed (putamen – green, globus pallidus – pink, caudate nucleus – blue, thalamus – brown, amygdala – red, hippocampus - yellow) b) last echo gradient echo magnitude image c) R_2^* map d) susceptibility (χ) map calculated with the optimised weak harmonic QSM method.

Neuropsychological Testing

People with TLE underwent neuropsychological tests providing measures of: verbal comprehension (vocabulary and similarity subtests of the Wechsler Adult Intelligence Scale; WAIS), working memory (digit span and arithmetic subtests of the WAIS), information processing (coding and matrix reasoning subtests of the WAIS), letter and category fluency, visual confrontation naming (McKenna Graded Naming Test), verbal and visual learning and recall (list and design A1-A5 and A6 subtasks of the BIRT Memory and Information Processing Battery; BMIPB). A comprehensive description of these neuropsychological tests has been provided elsewhere[30].

Comparison of QSM Methods

For all subjects, a total field map and a noise map were obtained from a non-linear fit of the complex SWAN data over all echo times[31,32]. Residual phase wraps were removed with Laplacian unwrapping[32,33] and a brain mask was obtained via Otsu thresholding[34] on the final echo of the SWAN magnitude images. The final echo was chosen as it provides a conservative brain mask estimate, removing regions of signal dropout near areas of high susceptibility gradients. To remove other noisy regions, the brain mask was eroded via thresholding at the mean of the inverse noise map[32,35,36] except within ROIs. To account for oblique slice acquisition, the total field map was rotated into alignment with the scanner axes, using FSL FLIRT[37] with trilinear interpolation, after phase unwrapping and prior to BFR[38]. The brain mask was then eroded by three voxels to improve the performance of BFR using projection onto dipole fields (PDF)[39].

The clinical multi-echo SWAN data were acquired using a sequence optimised for susceptibility weighted imaging (SWI) with parameters that were not appropriately optimised for QSM, which is a common issue for QSM analyses on retrospectively acquired clinical data. Acquired volumes had particularly high non-isotropic, spatial resolution and suffered from low signal-to-noise ratio (SNR) per volume, as well as residual background fields[40]. Therefore, to reduce the impact of noise and residual background field artefacts, susceptibility maps calculated using three separate local field-to-susceptibility inversion methods were compared. There are a range of dipole inversion methods to choose from and, after comparison of several state-of-the-art direct and iterative methods, iterative Tikhonov regularisation[41], non-linear total variation[42] and weak harmonic QSM (WH-QSM)[43] were selected. Iterative Tikhonov was chosen for its applicability to head (and neck) imaging[41] and its use in clinical QSM research[44,45]. Total variation-based approaches were shown to be the most accurate in the QSM Challenge 2.0[15] and non-linear total variation (FANSI), in particular, was chosen because it scored the highest in Stage 2 of the Challenge. WH-QSM was also investigated due to its additional ability to remove residual background fields. Further information for each method is given below.

Iterative Tikhonov Regularisation

The first method, iterative fitting with Tikhonov regularisation[41], was chosen as it has shown high repeatability in head and neck images[41]. It aims to minimise the energy of susceptibility solutions by solving the minimisation problem

$$\arg\min_{\chi} \| MW(\Delta B_z(r) - B_0 \chi(r) * d_z(r)) \|_2^2 + \alpha \|\chi\|_2^2, \tag{2}$$

where the first term is the data fidelity term reflecting the difference between the forward field calculation and the measured MRI signal, $\Delta B_z(r)$ is the measured local magnetic field, B_0 the magnetic field strength, $d_z(r)$ the unit magnetic dipole, $\chi(r)$ is the tissue susceptibility distribution, M is the brain mask, W (the reciprocal of the noise map) is a weighting term accounting for spatially varying noise, and α is the Tikhonov regularisation parameter. The latter was set to $\alpha = 0.0652$ by averaging the results of an L-Curve analysis in ten randomly selected subjects[46].

Non-Linear Total Variation

The second method, non-linear total variation (TV), scored highly in the QSM Challenge 2.0[15]. It solves a non-linear version of Equation 2, moving from a Gaussian noise representation to a more realistic complex-valued Gaussian noise distribution for MRI measurements[47], with TV regularisation which promotes piece-wise constant solutions:

$$\arg\min_{\chi} \left\| W\left(e^{i(B_0\chi(r)*d_z(r))} - e^{i\Delta B_z(r)}\right)\right\|_2^2 + \alpha|\nabla\chi|_1 . \qquad (3)$$

Equation 3 was solved using the FANSI toolbox[29,42,48] with the default convergence tolerance (0.1). The regularisation parameter $\alpha = 1.956 \times 10^{-5}$ was chosen by averaging the results of an L-Curve and frequency spectrum analysis[49] in the same ten subjects as for iterative Tikhonov regularisation.

Weak Harmonic Non-Linear Total Variation

The third method, known as Weak-harmonic (WH) QSM, contains an additional regularisation term to remove residual background field artefacts[43]. This solves the minimisation problem

$$\arg\min_{\chi,\phi_h} \left\| W\left(e^{i(B_0\chi(r)*d_z(r)+\phi_h(r))} - e^{i\Delta \mathrm{B_z}(r)}\right)\right\|_2^2 + \frac{\beta}{2}\|M\nabla^2\phi_h\|_2^2 + \alpha|\nabla\chi|_1, \qquad (4)$$

which is the same as equation 3 but with an additional WH term, where ϕ_h contains residual background fields after BFR with PDF. These fields are forced to be harmonic through the WH penalty term, with β as the WH regularisation parameter, which was set to the default value (150). This value was empirically checked to ensure that only residual background fields, and no anatomical information, were contained within the harmonic field maps ϕ_h. As in the non-linear TV formulation $\alpha = 1.956 \times 10^{-5}$ was chosen.

Statistical Analyses

In all analyses, P<0.05 was used to determine statistical significance unless stated otherwise. Normality of the variables was tested using the Lilliefors goodness-of-fit test of composite normality, using P<0.01 to determine statistical significance. Comparison of demographic data between study groups was performed using the Kruskal-Wallis test for continuous variables (age, age at onset, seizure frequency) and the chi-square test for categorical variables (sex, history of status epilepticus, seizure type).

As χ and R_2^* are known to depend on age[50,51] and to account for possible age differences between groups, mean χ and R_2^* values in the ROIs were corrected for age. A linear age correction was chosen as there was large variability in ROI mean values and the quality of the linear fit was far greater than using an exponential model. Age-correction used a least-squares linear fit across control participants in each ROI[52], pooled across both hemispheres

$$\widehat{Y}_i = \lambda_i + \theta_i A \tag{5}$$

where $\widehat{Y}_i$ is the mean value (χ or R_2^*) in an ROI i, A is the age, and λ_i and θ_i are the fitted parameters. The age-corrected mean value in each ROI i and TLE subject j, $\chi_{i,j}$, is given by:

$$\chi_{i,j} = Y_{i,j} + \theta_i(\mu - A_j) \tag{6}$$

where $Y_{i,j}$ is the measured mean value, μ is the mean age in the control group, and A_j is the age of subject j.

QSM Quality

To quantitatively compare the noise levels within ROIs of susceptibility maps calculated using the three different inversion methods, the standard deviation of χ was calculated in each ROI of each subject and a three-group two-tailed ANOVA was performed to compare the average standard deviation between the three susceptibility calculation techniques: iterative Tikhonov regularisation, non-linear TV and WH-QSM.

Comparing ROI mean χ and R_2^* Between Groups and Hemispheres

Three-group two-tailed ANOVA was then performed for each ROI, testing for significant differences in χ and R_2^* values between the LTLE, RTLE and control groups, using η^2 to denote the effect size. Post-hoc Tukey-Kramer tests were used to assess which groups exhibited statistically significant differences if ANOVA revealed group differences, which incorporates multiple comparison correction. Here, Cohen's d is used to denote the effect size. Additionally, intra-subject left-right differences in ROI mean values were investigated per group using a paired t-test, using Cohen's d to denote the effect size.

To ensure any regional differences found were not driven by age, individual linear fits of χ/R_2^* versus age for the three groups were compared using analysis of covariance in all ROIs (pooled across both hemispheres).

Correlation with Clinical Features

In TLE, age of onset is correlated with various MRI-based biomarkers (e.g., cortical thinning[5]) so we explored correlations between ROI mean susceptibility and R_2^* and age of onset. Age of epilepsy onset was distributed highly non-normally, and as log-transformation did not improve this we used Spearman rank correlations to investigate correlations with susceptibility or R_2^*.

Previous work in TLE indicates that the thalamus and basal ganglia may facilitate FBTCS[8,9]. Therefore, we compared ROI mean susceptibility and R_2^* across patient groups stratified based on FBTCS (none, historic, or recent) using ANOVA. In those patients with recent FBTCS we also correlated these quantitative measures with frequency of FBTCS in the year preceding the scan[9] using Pearson correlation. As only 7 LTLE and 8 RTLE patients reported recent FBTCS, data from the two patient groups were pooled by ipsilateral and contralateral ROIs, as the impact of FBTCS is considered as most prominent in the ipsilateral hemisphere[8,9].

Neuropsychological test scores were correlated with the ROI mean susceptibility and R_2^* using multiple linear regressions to include covariation with patient group (LTLE vs RTLE). For some cognitive test scores, it is known that LTLE and RTLE are affected differently[53,54], therefore, we included an interaction term between patient group and cognitive test. Some cognitive processes (e.g., naming) rely on lateralized hemispheric processing, so left-sided and right-sided ROIs were considered in separate regressions. These regressions can reveal if imaging metrics correlate with cognitive scores (slope of regression), if the two groups (LTLE and RTLE) have a difference in average susceptibility/ R_2^* (group effect), or a different sign/magnitude of effect between the groups (group x cognitive score interaction). As not all participants performed all tests, the number of participants included in each correlation analysis is given with the statistical test outcomes. Based on prior work highlighting the relevance of the thalamus and basal ganglia for linguistic and executive processing[53–55], executive function tests (working memory, arithmetic, picture naming, and letter and category fluency) as well as information processing and verbal comprehension scores were included in a multiple regression model with the ROI mean susceptibilities or R_2^* values within the caudate nucleus, hippocampus, GP, putamen, and thalamus. Finally, verbal and visual memory scores were regressed against mean hippocampal susceptibility and R_2^* values. These regressions were deemed significant at P<0.05 using the false discovery rate to correct for multiple comparisons.

In each group, we performed correlations between hippocampal volume – a known radiological biomarker of HS – and mean hippocampal χ values and between hippocampal volume and mean R_2^* values to investigate if these susceptibility-based metrics provide overlapping or new information.

Data Availability

The data that support the findings of this study are available upon reasonable request from the corresponding author.

Table 1: **Demographic information for each group**

	Healthy controls (n=27)	Left TLE (n = 19)	Right TLE (n = 17)
Age range; median (IQR), years	16.5-55.1; 30 (9.6)	19.4-66.5; 32.9 (15.9)	21.4-67.1; 34.0 (16.3)
Sex female/male, n	9/18	7/12	8/9
Surgery yes/no, n	N/A	7/12	2/15
Age at onset[a] median (IQR), years	N/A	10.0 (16.5)	15.0 (16)
Epilepsy duration[a] median (IQR), years	N/A	25.8 (29.9)	18.0 (21.2)

History of SE yes/no/unknown, n	N/A	1/8/10	2/8/7
FAS yes/no/unknown, n	N/A	10/3/6	7/2/8
FIAS yes/no/unknown, n	N/A	14/0/5	15/1/1
FBTCS Recent/historic/none	N/A	7/8/4	8/5/4
FBTCS frequency[b] Median (IQR), per month	N/A	0.75 (0.65)	2.50 (4.0)

Abbreviations: FAS: focal aware seizures; FBTCS: focal-to-bilateral tonic-clonic seizures, with 'recent' meaning within the last 12 months, 'historic' means ever but not in the last 12 months; FIAS: focal impaired aware seizures; IQR = inter-quartile range; SE: status epilepticus; TLE: temporal lobe epilepsy.
[a]indicates missing data (4 for left TLE, 2 for right TLE)
[b]indicates missing data (12 for left TLE, 9 for right TLE)

Results

Demographic and Clinical Characteristics

There was a significant difference in age between the three groups (Table 1; $\chi^2 = 7.96$; $df = 2$; $P = 0.019$, $\eta^2 = 0.12$), and susceptibility values were age-corrected as detailed above. Sex was not different between the three groups. None of the other patient characteristics were significantly different between left and right TLE groups. All surgical specimens were HS type 1.

QSM Quality

Susceptibility maps calculated via iterative Tikhonov regularisation suffered from noise and residual background fields, particularly in the cerebellum and the top of the brain (Figure 2). Upon visual comparison, non-linear TV reduced noise and increased the contrast in deep grey matter ROIs (Figure 2). Residual background fields remained in the non-linear TV susceptibility maps, and WH-QSM qualitatively reduced the noise, reduced the standard deviation of susceptibility values within ROIs, and removed residual background fields (Figure 2).

Three-group one-way ANOVA indicated significant standard deviation differences between the three susceptibility calculation methods in the bilateral caudate nucleus ($P <$

0.001 for both), putamen ($P < 0.001$ for both), thalamus ($P < 0.001$ for both), hippocampus ($P < 0.001$ for both), and left GP ($P = 0.021$). Tukey-Kramer multiple comparison analysis tests revealed that non-linear TV had significantly greater standard deviation in several ROIs (Figure 3) compared to both iterative Tikhonov and WH-QSM. It also revealed that WH-QSM outperformed both non-linear TV and iterative Tikhonov in all of ROIs that displayed significant differences across methods except for the left GP, where it only outperformed non-linear TV (Figure 3).

This quality comparison identified WH-QSM as the optimal method for these data and all group results and correlations shown are from the susceptibility maps calculated with WH-QSM.

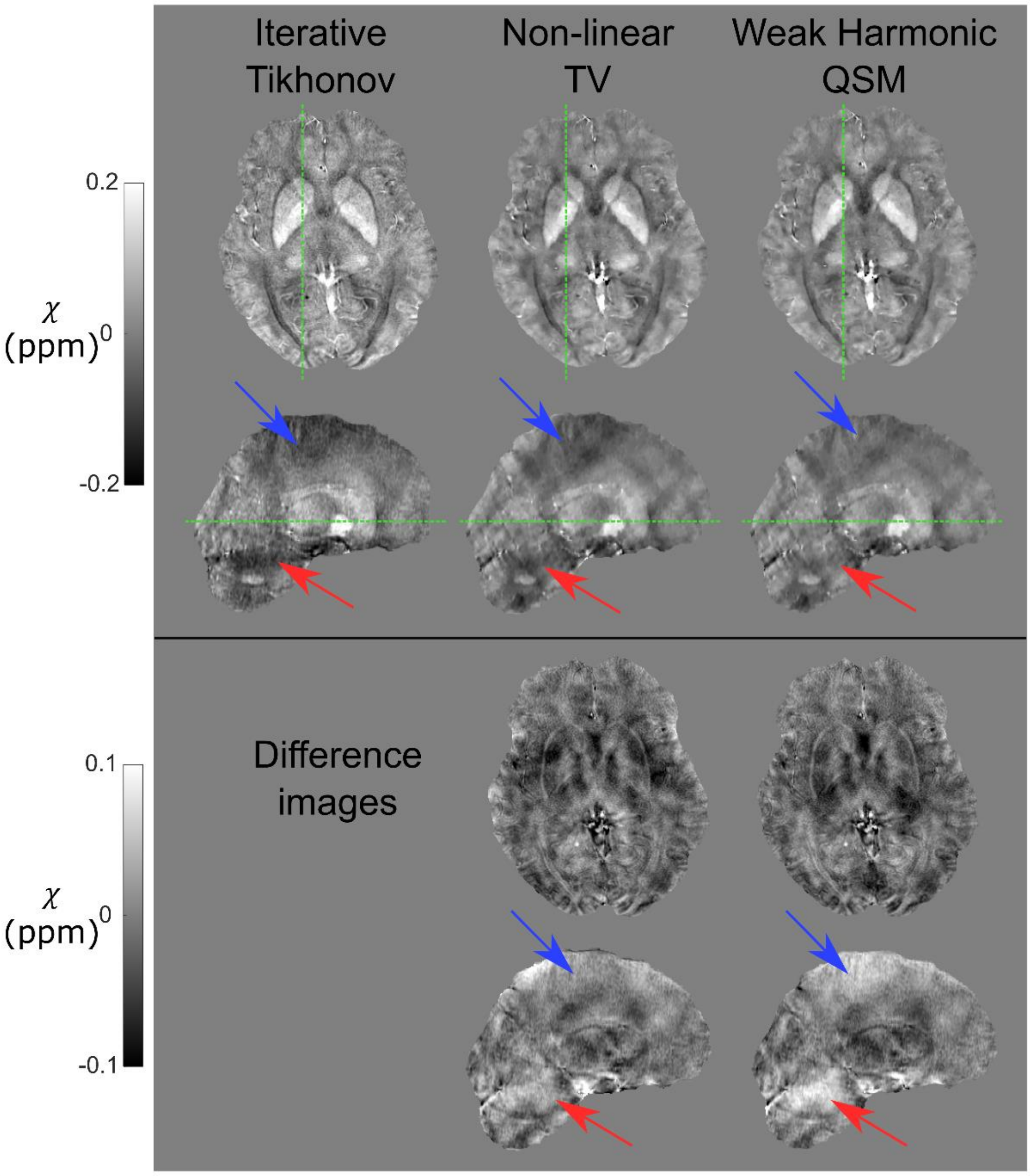

Figure 2: Comparison of susceptibility calculation techniques. Comparison of the three susceptibility (χ) calculation methods in a representative RTLE subject: iterative Tikhonov regularisation (left), non-linear total variation (middle) and weak harmonic QSM (right). Difference images are relative to the iterative Tikhonov regularisation susceptibility map. Iterative Tikhonov suffers from high noise and residual background fields. WH-QSM performs the best, removing both noise and residual background fields. This is most evident in the cerebellum (red arrows) and the top of the brain (blue arrows). Axial and sagittal slice positions are indicated by the green dashed lines.

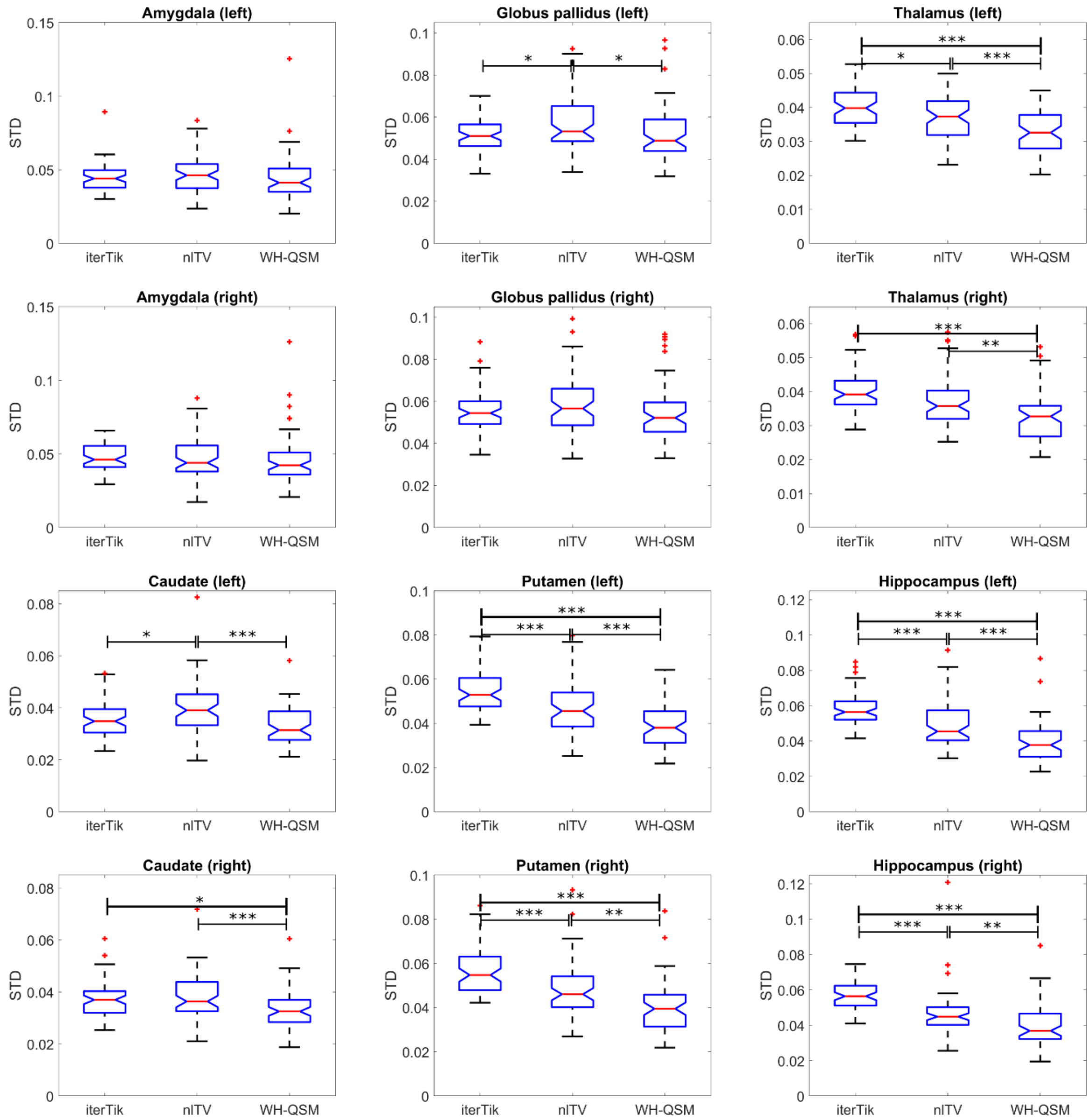

Figure 3: Comparison of standard deviation across susceptibility calculation techniques. The average standard deviation of susceptibility values in each ROI, over all participants regardless of disease state, was compared across the three QSM methods: iterative Tikhonov regularisation (iterTik), non-linear total variation (nlTV) and weak harmonic QSM (WH-QSM). WH-QSM consistently had the lowest standard deviation for all ROIs. An outlier (STD > 0.25) in the left and right amygdala in the non-linear TV group has been omitted to facilitate comparison. * indicates $P < 0.05$, ** indicates $P < 0.01$, *** indicates $P < 0.001$.

Group Differences in Susceptibility

The susceptibility values in all ROIs in all groups were found to be normally distributed. We observed significant susceptibility differences between groups in the left hippocampus ($P = 0.020$), right thalamus ($P = 0.049$), left putamen ($P = 0.036$) and the right putamen ($P = 0.017$) using ANOVA (Figure 4, Supplementary Table 1). Tukey-Kramer multiple comparison analysis tests revealed that: the LTLE group had a significantly lower susceptibility in the left hippocampus compared to healthy controls ($P = 0.015$), but the RTLE group did not ($P = 0.513$). The RTLE group had a significantly higher susceptibility in the right thalamus than healthy controls ($P = 0.040$), but the LTLE group did not ($P = 0.757$). The RTLE group had a significantly higher susceptibility in the left putamen compared to the LTLE group ($P = 0.041$), and in the right putamen compared to healthy controls ($P = 0.014$). The LTLE group was not significantly different in susceptibility of the left putamen ($P = 0.859$) or the right putamen ($P = 0.789$) compared to healthy controls. Effect sizes and details can be found in Table 2.

We also identified left-right asymmetry in susceptibility in the putamen in the healthy control group, with the left putamen having a higher susceptibility than the right ($P = 0.032$) using a paired *t*-test. No asymmetry in putamen susceptibility was observed in the LTLE or RTLE groups. Although no left-right asymmetry in susceptibility was found in the hippocampi in any of the groups, subgroup analysis within the surgical LTLE group did reveal a significantly lower susceptibility in the left (affected) hippocampus than the right (-0.050 ppm vs -0.035 ppm, respectively, $P = 0.031$).

No statistically significant differences between groups in the analysis of covariance of susceptibility with age were found in any of the ROIs (Supplementary Figure 3), indicating that the regional differences found were not driven by age.

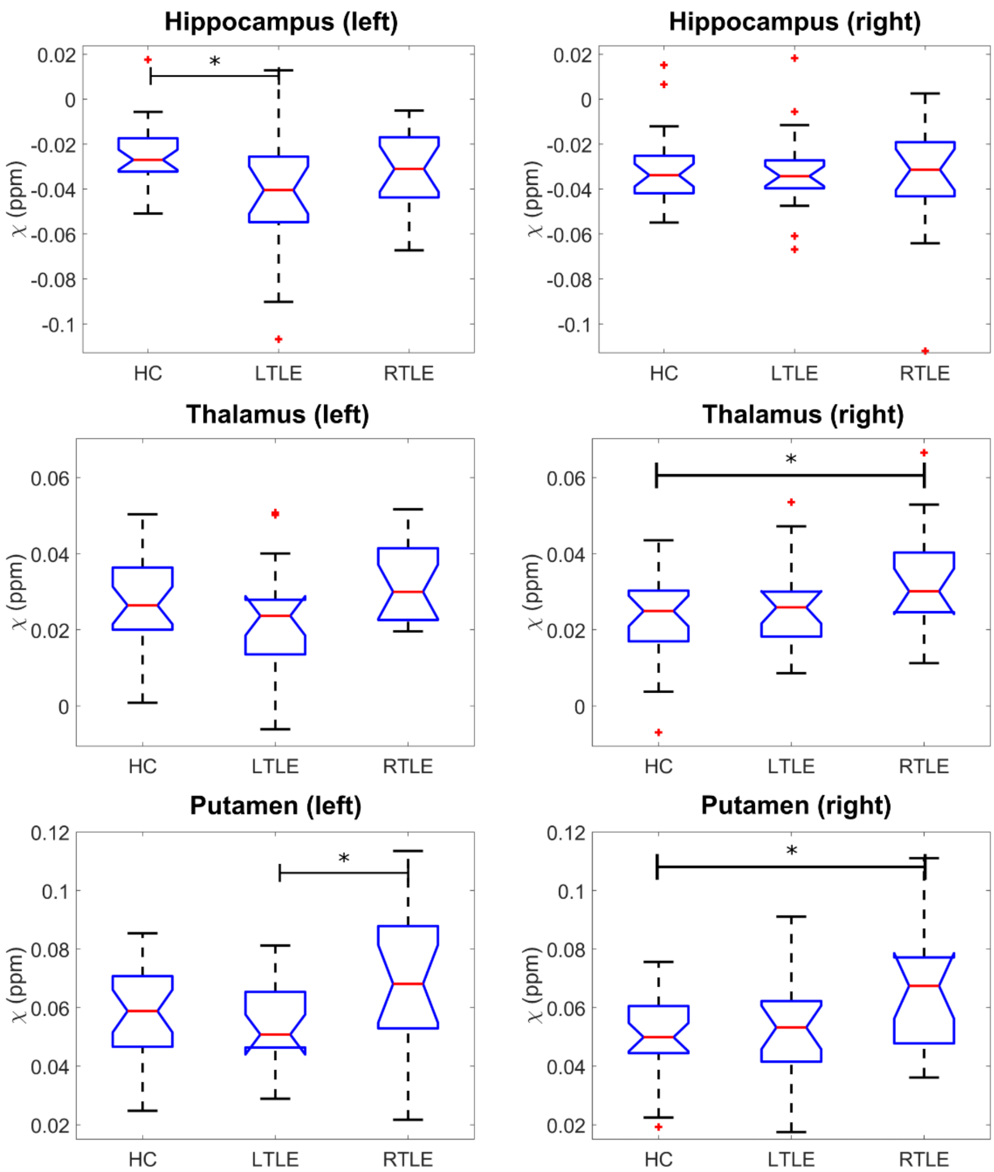

Figure 4: Significant ROI mean susceptibility differences between TLE and healthy control groups. Boxplots showing comparison of average susceptibility (χ) across the three groups. * indicates $P < 0.05$. Abbreviations: HC: healthy controls; LTLE: left temporal lobe epilepsy; RTLE: right temporal lobe epilepsy

Group Differences in R_2^*

The R_2^* values in all ROIs were found to be normally distributed. With ANOVA, we observed group R_2^* differences (Figure 5, Supplementary Table 1) in the left and right amygdala ($P = 0.0029$ and $P = 0.0063$, respectively), hippocampus ($P = 0.0012$ and $P < 0.001$, respectively), the left putamen ($P = 0.0078$) and the left thalamus ($P = 0.0069$).

Tukey-Kramer multiple comparison analysis tests revealed that both the LTLE and RTLE group had significantly lower R_2^* in the left amygdala compared to healthy controls ($P = 0.004$, $P = 0.031$, respectively). The TLE groups had significantly reduced R_2^* in their ipsilateral hippocampus compared to both healthy controls and the contralateral hippocampus (Figure 5). The left putamen was found to have a significantly higher R_2^* in the RTLE group compared to the LTLE group ($P = 0.005$) but not the control group. The left thalamus had a significantly higher R_2^* in the RTLE group than both the control and LTLE groups ($P = 0.049, P = 0.006$). Effect sizes and details can be found in Table 2.

Using paired *t*-tests, we also identified left-right asymmetry in the hippocampus of the LTLE and RTLE groups, with the ipsilateral hippocampus having a lower R_2^* than the contralateral hippocampus in each group ($P = 0.0215$ and $P = 0.0265$, respectively). We also identified asymmetry in the GP of the RTLE group with the left GP having a higher R_2^* than the right ($P = 0.0167$).

No statistically significant differences between groups in the analysis of covariance of R_2^* and age were found in any of the ROIs (Supplementary Figure 4), indicating that the regional differences found were not driven by age.

Table 2: Significant Results of ANOVA for group-wise χ and R_2^* comparisons. ANOVA p-values, post-hoc Tukey-Kramer (T-K) p-values and their corresponding effect sizes (η^2 and Cohen's d, respectively) for group-wise χ and R_2^* comparisons, which showed significant ANOVA differences. Bold table entries signify statistically significant differences (with post-hoc T-K p < 0.05).

Susceptibility (χ)			HC v LTLE		HC v RTLE		LTLE v RTLE	
ROI	ANOVA	η^2	T-K p-value	Cohen's d	T-K p-value	Cohen's d	T-K p-value	Cohen's d
Hippocampus (left)	0.020	0.122	**0.015**	**0.837**	0.513	0.418	0.269	0.433
Putamen (left)	0.036	0.105	0.859	0.186	0.084	-0.623	**0.041**	**0.726**
Putamen (right)	0.017	0.127	0.789	-0.212	**0.014**	**-0.893**	0.098	0.614
Thalamus (right)	0.049	0.096	0.757	-0.222	**0.040**	**-0.742**	0.221	0.527
R_2^*								
Amygdala (left)	0.003	0.177	**0.004**	**1.054**	**0.031**	**0.854**	0.838	0.158
Amygdala (right)	0.006	0.155	0.262	0.539	**0.004**	**1.011**	0.232	-0.465
Hippocampus (left)	0.001	0.202	**0.001**	**1.207**	0.904	0.136	**0.013**	**0.831**
Hippocampus (right)	0.0001	0.256	0.347	0.573	**0.0001**	**1.289**	**0.013**	**-0.797**
Putamen (left)	0.008	0.149	0.195	0.584	0.177	-0.514	**0.005**	**1.004**
Thalamus (left)	0.007	0.153	0.527	0.308	**0.049**	**-0.839**	**0.006**	**0.958**

Abbreviations: ROI: region of interest; HC: healthy controls; LTLE: left temporal lobe epilepsy; RTLE: right temporal lobe epilepsy

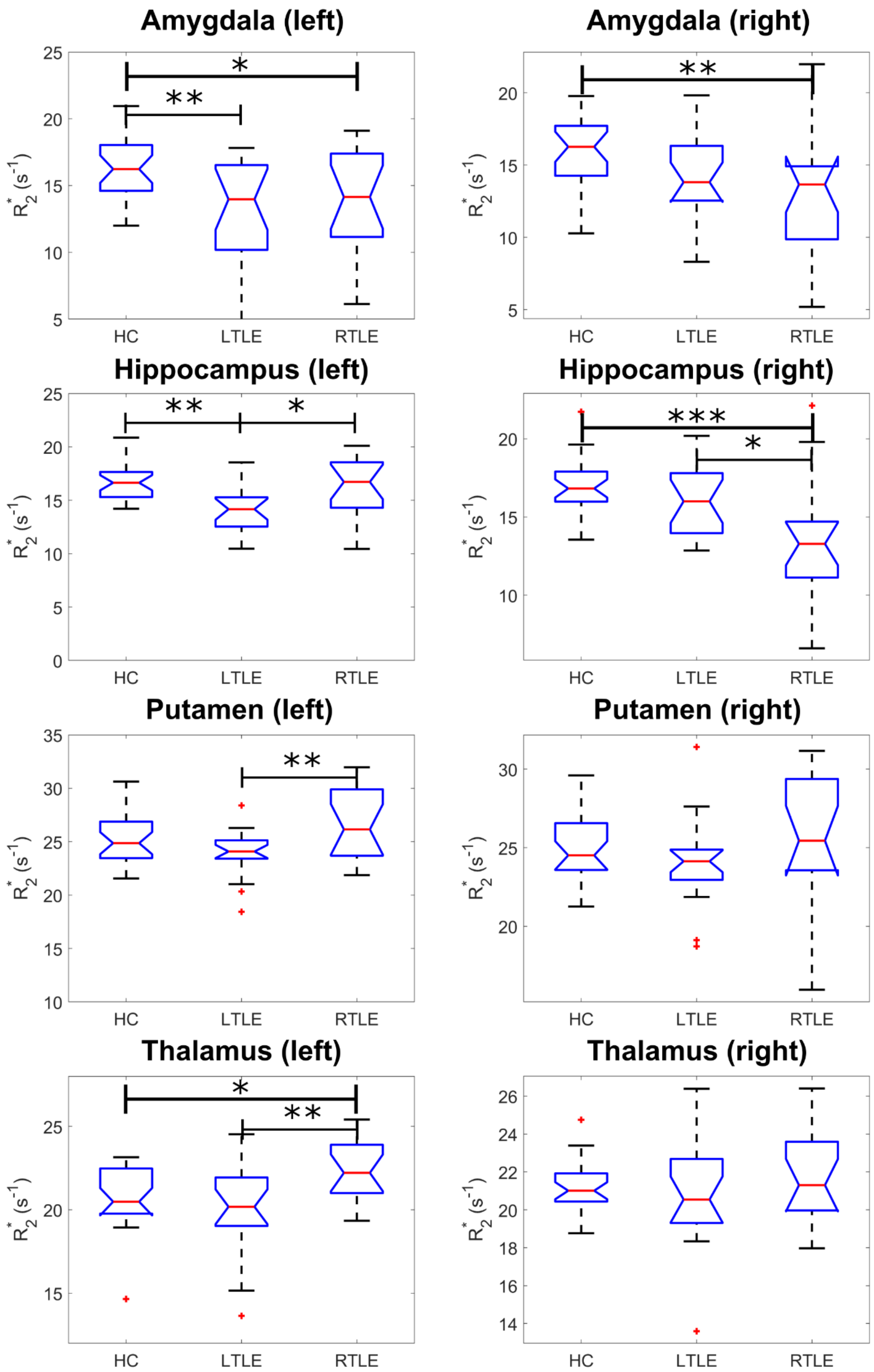
Amygdala (left)
Amygdala (right)
Hippocampus (left)
Hippocampus (right)
Putamen (left)
Putamen (right)
Thalamus (left)
Thalamus (right)
$R^*_2\ (s^{-1})$
HC
LTLE
RTLE
*
**
***

Figure 5: Significant ROI mean R_2^* differences between TLE and healthy control groups. Significant R_2^* group changes in six ROIs are shown. Both pathological hippocampi in their respective TLE group were found to have significantly reduced R_2^* values. * indicates $P < 0.05$, ** indicates $P < 0.01$, *** indicates $P < 0.001$.

Correlations with Clinical Features

We found negative correlations between age of TLE onset and: bilateral putamen susceptibility ($P = 0.013$ for left; $P = 0.028$ for right) and right hippocampal susceptibility ($P = 0.014$) in the LTLE group. A positive correlation was found between the age of TLE onset and left caudate R_2^* ($P = 0.034$) in the RTLE group (Figure 6).

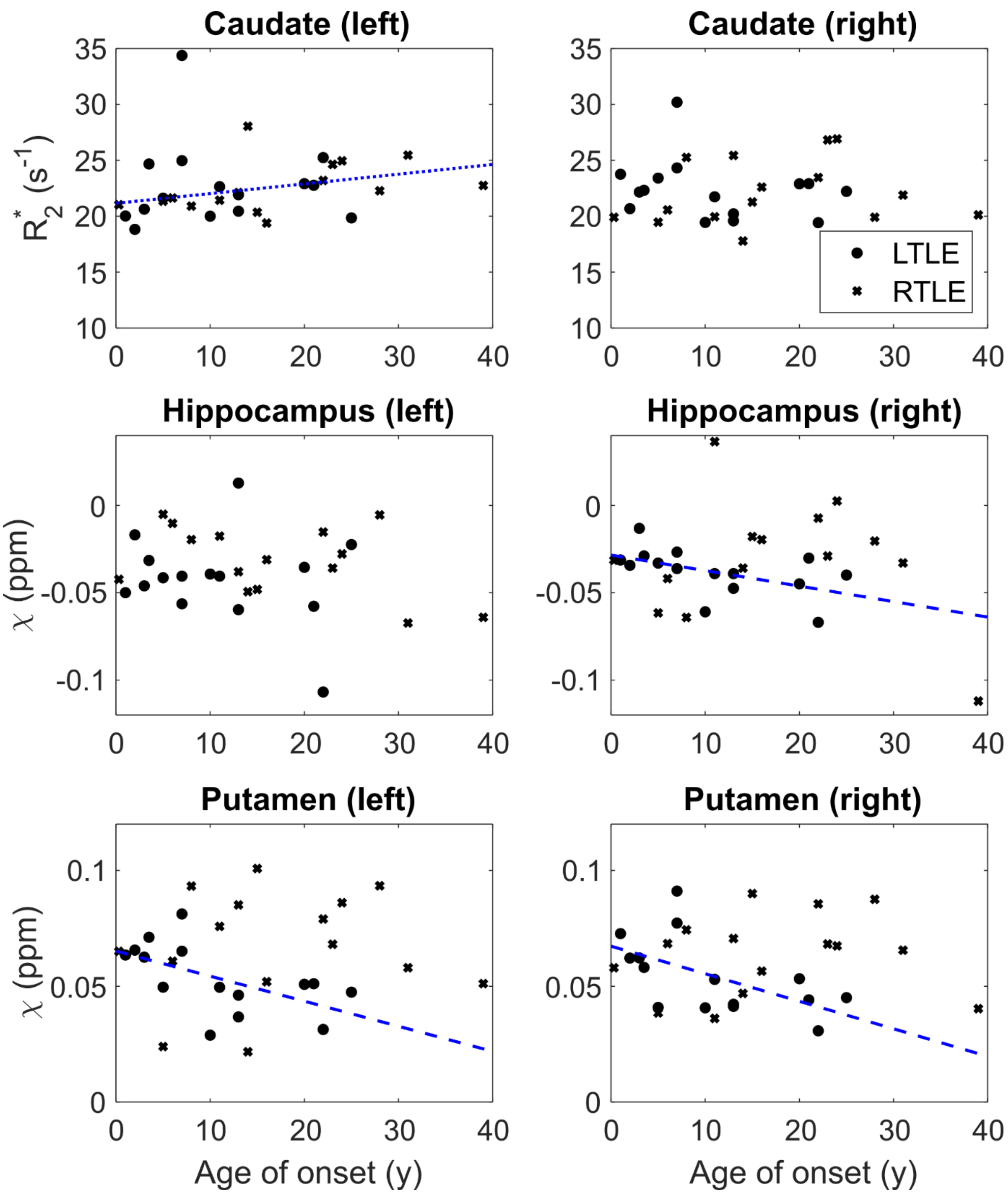

Figure 6: Susceptibility and R_2^* versus age of TLE onset. Scatterplots showing caudate R_2^* and hippocampal and putamen susceptibility (χ) versus age of TLE onset. Dots indicate people with left temporal lobe epilepsy (TLE); crosses indicate people with right TLE. Dashed (left TLE) and dotted (right TLE) lines indicate plots of linear correlation for regions with significant correlations. These lines are shown only as a visual aid as significance testing was performed using Spearman rank correlation.

There were no significant differences in susceptibility or R_2^* between FBTCS groups (recent, historic, or none). FBTCS frequency was highly non-normal ($P < 0.001$), and data were log-transformed to ensure normality ($P = 0.25$ after log-transformation) and facilitate linear correlations with χ and R_2^*. There were significant positive correlations between FBTCS frequency and susceptibility in the ipsilateral thalamus ($P = 0.031$) and the contralateral putamen ($P = 0.042$), and significant positive correlations between FBTCS frequency and R_2^* in the ipsilateral and contralateral globi pallidi ($P = 0.040$ and $P = 0.036$, respectively; Figure 7).

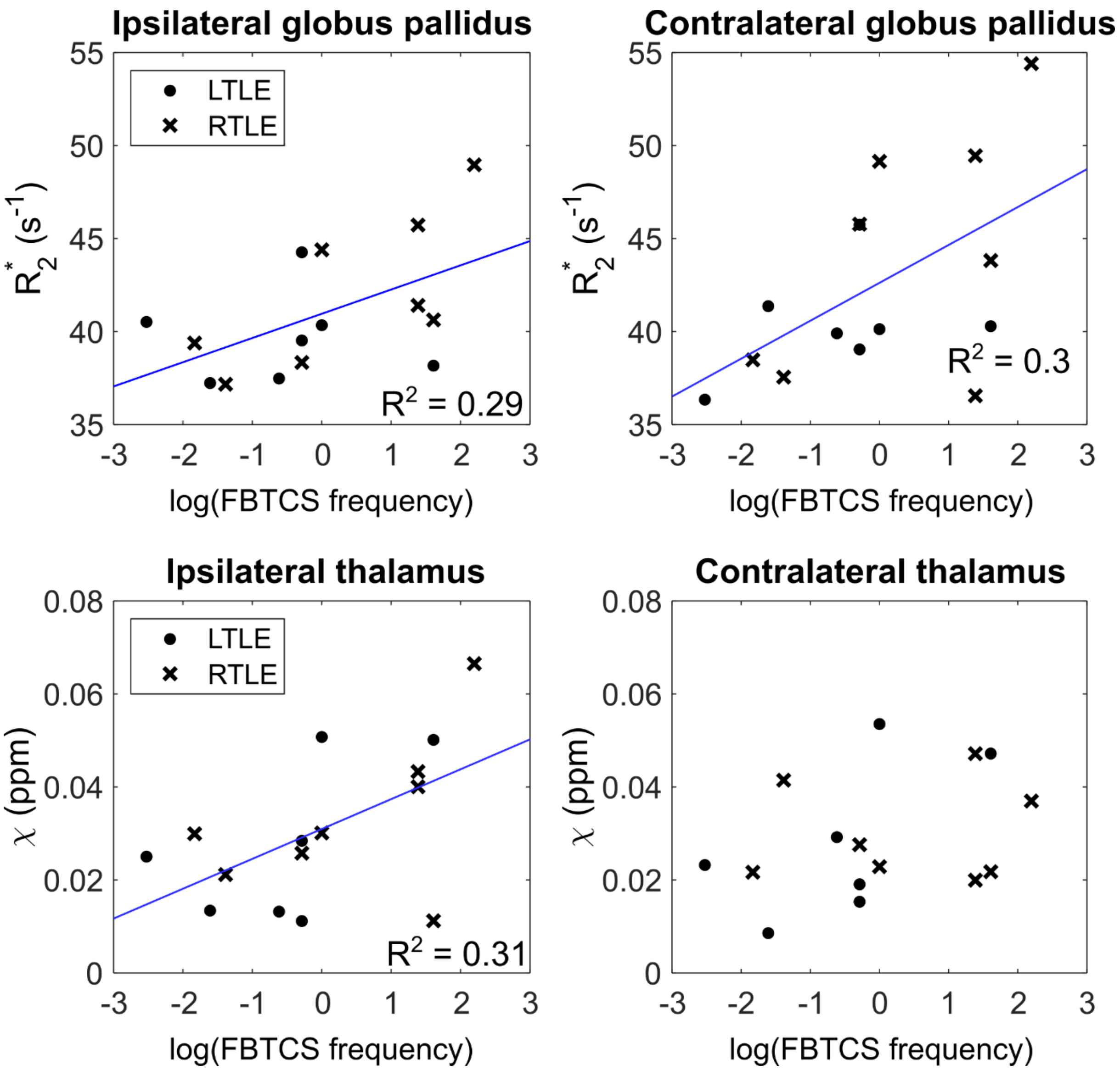

Figure 7: Susceptibility and R_2^* versus log-transformed frequency of FBTCS. Scatterplots showing thalamic and putamen susceptibility (χ) and R_2^* in the globi pallidi against the frequency of focal to bilateral tonic-clonic seizures (FBTCS), log-transformed to ensure

normality. Dots indicate people with left temporal lobe epilepsy (TLE); crosses indicate people with right TLE; the black line indicates the linear fit of significantly correlated factors.

None of the neurocognitive test scores were significantly correlated with age for either patient population. Significant multiple linear regressions between neuropsychological tests and susceptibility or R_2^* are summarised in Supplementary Table 2. Neuropsychological scores were normally distributed for all tests. No significant findings were observed for the right-sided ROIs. Arithmetic performance (n=18) was associated with higher left caudate susceptibility ($P = 0.0032$) and higher left putamen susceptibility ($P < 0.001$). In both regions, the RTLE patients had higher susceptibility values, a difference that diminished with higher test scores (negative interaction). Letter fluency (n=32) was associated with higher left hippocampal R_2^* ($P = 0.0022$) and higher left thalamic R_2^* ($P = 0.0056$). For the hippocampus, RTLE patients had lower R_2^* values but a stronger increase in R_2^* with increasing test scores (positive interaction). For the thalamus, RTLE patients had a higher R_2^* that increased further with increasing test scores (a positive interaction term). Matrix reasoning (n=31) was positively associated with left thalamic R_2^* ($P = 0.029$). Here, the RTLE group had higher R_2^* values, but with a smaller positive association between test scores and R_2^* (a negative interaction). No correlations were observed for other regions or other cognitive test scores.

Investigations of correlations between hippocampal susceptibility or R_2^* and volume found a significant positive ($P = 0.036$) association between hippocampal volume and R_2^* in the right hippocampus in the RTLE group (Supplementary Figure 2).

Discussion

In this study, we investigated the use of QSM in a cohort of people with TLE and healthy controls. We revealed, for the first time, that there are *in vivo* susceptibility and R_2^* differences between people with TLE and healthy controls in the amygdala, hippocampus, thalamus, and basal ganglia. We also identified correlations between susceptibility and R_2^* measures and clinical characteristics (age at epilepsy onset, FBTCS frequency in the last year, and neuropsychological test scores), indicative of these quantitative MRI metrics' sensitivity to changes in tissue composition underlying disease characteristics and cognitive performance.

To provide a biological interpretation of the observed χ and R_2^* changes, it is important to consider what these measures reflect. χ estimates reflect the magnetic susceptibility which, in biological tissues, is primarily influenced by myelin and iron content[56]; myelin is diamagnetic (χ<0, meaning that myelin reduces the local magnetic field strength), while iron is paramagnetic (χ>0, meaning iron enhances the local magnetic field). However, when χ increases are observed, these could be the result of myelin reduction or iron accumulation. R_2^* complements χ measurements, as R_2^* is a measure of the concentration of microscopic susceptibility sources, with R_2^* increases indicating an increase in susceptibility sources (e.g., increased tissue iron). This means that an observed increase in both χ and R_2^* in a particular brain region is most parsimoniously explained by an increase in paramagnetic iron content in that region, whereas an increase in χ coupled with a reduction in R_2^* are more indicative of reduction in diamagnetic myelin content. Other factors may contribute to χ and R_2^* (e.g., zinc, calcium), and therefore, without histological confirmations, the above interpretations may still reflect a simplification of the true biological complexity.

Regional Differences Between Groups

In people with LTLE, the left hippocampus had a significantly lower susceptibility than in the controls, and a lower mean R_2^* than the right hippocampus. In the RTLE group, R_2^* values were significantly lower in the right hippocampus than the left in agreement with literature[10]. Group differences may be explained by the observed within-subject asymmetry, with both patient groups demonstrating lower ipsilateral than contralateral R_2^*. Further, there is a consistently more negative ipsilateral hippocampal susceptibility in the subgroup of LTLE patients who underwent surgery. Right hippocampal volume was positively correlated with right hippocampal R_2^*, indicating that, with more atrophy, there was a reduction in R_2^* and thus a loss of susceptibility sources (e.g., myelin or iron). Hippocampal susceptibility differences were not found in the RTLE group, possibly due to a slightly smaller sample and higher within-group standard deviation (0.0313 ppm vs 0.0265 ppm).

Although a loss of hippocampal iron might be postulated as the simplest cause of these susceptibility and R_2^* decreases, this may at first glance be complex to reconcile with the underlying biology, given that the two main histopathological hallmarks of HS are neuronal cell loss and gliosis[57]. Neuronal cell loss, especially in HS type 1 as observed in our participants, predominantly affects CA1 and spares the subiculum[57]; the latter is heavily myelinated, especially compared to CA1[58,59]. Hence, we hypothesize that a loss of relatively low-myelinated neurons in CA1 may increase the average myelination (i.e. the concentration of diamagnetic myelin) throughout the hippocampus and thus explain the decreased susceptibility values in the affected left hippocampi.

Significant decreases in R_2^* in the right hippocampus of the RTLE group and the correlation between R_2^* and hippocampal volume in the same RTLE group point towards demyelination accompanied by neuronal cell loss – because R_2^* decreases when tissue susceptibility sources (whether diamagnetic or paramagnetic) are lost. The left hippocampus in the LTLE group also shows a decrease in R_2^*, indicating the same mechanism, although the latter may be confounded by the significant susceptibility decrease in the pathological hippocampus of the LTLE group. Normally, we would expect demyelination (loss of diamagnetic myelin) to be observed as an increase in susceptibility, and highly myelinated regions with negative susceptibility to thus become less negative. However, as we explained above, the decrease in hippocampal susceptibility in the LTLE group together with a decreased R_2^* could be explained by a loss of low-myelinated CA1 neurons that leaves behind the subiculum's highly myelinated neurons.

Previous studies in multiple sclerosis[60] have also suggested that R_2^* and susceptibility changes can be explained by selective loss of particular cells (e.g. iron-rich versus iron-free cells or, in this study, low-myelin versus high-myelin neurons). Decreases in hippocampal susceptibility were also observed in premanifest Huntington Disease patients, and attributed to a possible redistribution of brain iron in response to the loss of myelin.[61] Harrison et al. further observed that a combined decrease in iron and myelin content can result in R_2^* decreases and unchanged susceptibility in multiple sclerosis.[62] Therefore, it seems that the R_2^* and susceptibility decreases we observed in the left hippocampus of the LTLE group could be a result of a complex interplay between loss of myelinated neurons (demyelination) and brain iron redistribution/dysregulation in this region. This is supported by a recent study into iron dysregulation in TLE which found histopathological evidence for iron deposition as well as dysregulation in the hippocampi of TLE patients[23] resulting in more extra-axonal iron, with iron binding and oxidative states also known to impact on susceptibility[63].

Importantly, we also identified correlations between markers of hippocampal tissue composition and cognitive test scores. Left hippocampal R_2^* was significantly correlated with letter fluency with lower R_2^* being associated with lower (worse) cognitive test scores, suggesting that the degree of pathological change in hippocampal composition may directly relate to multidomain cognitive impairment. In the LTLE group, who had lower group-wise left-hippocampal R_2^* (Figure 5), the effect of this cognitive score on R_2^* was reduced. These effects are in agreement with prior imaging work that suggests the importance of a hippocampal contribution to letter fluency[64].

In the amygdala, bilateral and ipsilateral decreases in R_2^* were observed in RTLE and LTLE compared to controls, respectively, suggestive of demyelination. The lack of significant susceptibility differences here may be attributed to the large within-subject and inter-subject variance in χ in this region (Supplementary Table 1). The amygdala is located very anteriorly in the mesial temporal lobe and is at the border between brain and non-brain tissue antero-medially. From a methodological perspective, the large variance in susceptibility in this region could be ascribed to technical factors, as BFR is known to be imperfect in the border region[40]. In TLE, the amygdala is a known structure of interest[65], with volumetric[66] and T2 relaxometry[67] abnormalities that reflect partial sclerosis[68]. Moreover, resection of the amygdala during temporal lobe surgery may lead to improved surgical outcomes[69]. All this points to similar pathological changes in the amygdala as the hippocampus, reflected by a similar R_2^* decrease in these two regions.

The right thalamus had significantly higher susceptibility values in RTLE compared to controls. The positive correlation of FBTCS frequency, a clinical marker of TLE severity, with the susceptibility in the ipsilateral thalamus is concordant with these changes. R_2^* measurements indicated abnormalities in the left thalamus in this RTLE group, with increased R_2^* indicating increased magnetic susceptibility sources. The observed increased thalamic susceptibility and R_2^* increases found here indicate that iron deposition is the most parsimonious explanation.

Left thalamus R_2^* values were positively correlated with matrix reasoning, consistent with demyelination affecting cognitive performance. The elevated susceptibility and R_2^* values in the ipsilateral thalamus in RTLE are more consistent with iron deposition than demyelination, indicating either disparate processes between hemispheres or multiple co-occurring pathological processes.

Thalamic changes are widely reported in TLE, including atrophy[4], diffusion MRI abnormalities[70], and reorganization of functional[8,9,71] and structural connectivity patterns[72]. Our findings advance our understanding of thalamic abnormalities in TLE, by indicating tissue composition changes. Further investigations would be required to explore relationships with abnormalities observed in these other imaging features, and to clarify the biological underpinnings. A complicating factor in thalamic QSM is the great intra-thalamic variability in susceptibility, with both myelinated and unmyelinated axons, and different cellular composition of the thalamic nuclei[73]. Given the small sample size and relatively low SNR of our data, we consider our findings best interpreted as exploratory. Future work leveraging larger sample sizes is advocated to better establish the underlying drivers of thalamic susceptibility changes.

In the putamen, the RTLE group had a significantly higher susceptibility compared to controls in the right putamen, and a higher susceptibility compared to the LTLE group in the left putamen. There was further evidence of differences between controls and TLE patients, in that there was a significant left-right asymmetry in healthy controls, concordant with higher iron content in the left than right putamen[74]. This asymmetry was not identified in left or right TLE patients. However, an increase in R_2^* was found in the left putamen in the RTLE group compared to the LTLE group. These χ and R_2^* findings are consistent with iron deposition in the putamen in TLE. The putamen has previously been shown to be affected in TLE patients, with smaller putamen volume bilaterally compared to healthy controls[75].

A within-subject asymmetry in R_2^* in the GP was observed in the RTLE group, with the left GP having higher R_2^* values than the right, and comparison with values from controls (Supplementary Table 1) indicates that indeed the left GP exhibits abnormally high R_2^*. This finding is in line with the increased R_2^* in the left thalamus and left putamen in the RTLE group. Higher right GP R_2^* was correlated with worse category fluency performance, which could be explained by iron deposition affecting local function. The GP was shown to be atrophic in TLE[76], and involved in an abnormal functional subnetwork with the putamen[8] and structural networks[77], showing structural and functional abnormalities in line with the R_2^* differences found here.

Correlations with Clinical Features

We observed significant positive correlations between left caudate R_2^* and age of epilepsy onset and significant negative correlations between χ in the hippocampus and putamen and age of onset. Considering χ and R_2^* correlations across these ROIs, this is consistent with reduced myelin content in those with earlier epilepsy onset.

We observed significant positive correlations between χ and R_2^* and FBTCS frequency in the thalamus and GP. These are the same regions found by He et al.[8] to have altered between-region functional interactions in those with recent FBTCS. As such, our results provide a possible structural hypothesis of increased iron deposition underpinning those previously observed functional changes.

Cognitive impairment, as captured by neuropsychological tests, is common in TLE and encompasses multiple domains, including memory, language, information processing, and executive function[78]. Here, we found that worse neuropsychological performance correlated with changes in mean χ and R_2^* in four regions of interest on three cognitive domains, with consistent correlations for information processing (left thalamus for matrix reasoning), executive function (letter fluency in left thalamus and left hippocampus), and working memory (arithmetic in left caudate and left putamen) all concordant with demyelination.

Impact

To the best of our knowledge, this is the first study to use QSM in TLE patients *in vivo* to investigate and quantify alterations in deep grey matter structures. Therefore, comparisons will be made with literature from other neurological conditions. Several other neurological disorders, including Alzheimer's, Parkinson's, and Huntington's diseases, are associated with widespread increases in susceptibility and R_2^* compared to controls that affect regions analysed in our work, including the amygdala, hippocampus, GP, thalamus, and putamen[61,79–81]. Given the well-characterised hippocampal abnormalities in this population of TLE with hippocampal sclerosis, we reason that the observed decreased hippocampal susceptibility is most likely a result of focal pathology. This is supported by the intra-subject asymmetry in susceptibility observed in the LTLE surgical subgroup alongside decreased R_2^* in pathological hippocampi compared to healthy contralateral hippocampi. Similar considerations apply to the reduced R_2^* in the amygdala[68]. Increased susceptibility and R_2^* observed in the putamen and thalamus in TLE suggest increased iron content in these regions. This is consistent with neurodegeneration studies where increased susceptibility in these regions was attributed to iron accumulation as part of the neurodegenerative process[79–81]. There is ongoing debate as to whether epilepsy is a neurodegenerative disease[82–84]. A recent meta-analysis[4] of MRI studies over the last two decades identified progressive cortico-subcortical grey matter loss in TLE, and recent longitudinal MRI work found progressive cortical thinning in people with focal epilepsy, including TLE, beyond that observed in healthy aging[5]. Hence, the results from our study could be interpreted as being consistent with this narrative. Further investigations are required to confirm or disprove such interpretation.

From a methodological perspective, we show that the difference in image quality between three susceptibility calculation methods – with WH-QSM performing best here – exemplifies the impact that non-optimized data processing can have on study results. Recent QSM challenges[15,16] have set out to ascertain which susceptibility calculation methods are most accurate and informed our choice of analysis methods. The top-scoring FANSI method[42], used with the reportedly most accurate TV-based regularisation that promotes piece-wise constant solutions, yielded higher variability in our data compared to an adapted version of FANSI with an additional weak-harmonic penalty term, WH-QSM[43]. This weak-harmonic penalisation was designed to remove residual harmonic background fields[43] and successfully did so for our data. Although there are ongoing efforts within the QSM research community to achieve consensus on the best QSM processing and susceptibility calculation methods[85], this study suggests that optimisation and choice of QSM reconstruction methods for particular datasets are necessary and beneficial, particularly when performing retrospective QSM reconstruction on data acquired using parameters that were not optimised for QSM – as in this study.

Limitations

A main limitation of this work is the low SNR of the data, which was a consequence of using routinely acquired susceptibility-weighted imaging data without QSM-optimised acquisition parameters. We addressed this by conducting an evaluation of three QSM methods to minimise artefacts and ensure robustness in our susceptibility estimates. Furthermore, our patient sample size was relatively small, and although it was exclusively a TLE-HS population, there was still within-group heterogeneity in terms of age of onset and seizure characteristics, such as FBTCS frequency, which we identified as associated with these susceptibility-based imaging measures. Given the limited sample size and novel use of QSM in TLE, we considered our work as an exploratory study and did not correct for multiple comparisons, but instead used a more stringent uncorrected p-value for the neuropsychological correlations. The consistency of our results – with matching χ and R_2^* changes across participant groups, consistent correlations across different tests per cognitive domain, and findings correlating with clinical features such as FBTCS characteristics and age of onset – indicate that these results reflect genuine changes in tissue composition in TLE. The lifespan trajectories of susceptibility and R_2^* with age are nonlinear[86], but a linear correction for age was selected because it provided the best fit to our data.

Although QSM and R_2^* changes may reflect and suggest changes in tissue composition, the findings of this study were all obtained from non-invasive in-vivo imaging; therefore, we can only speculate about the neuropathological substrates underpinning these imaging findings. Neuropathological studies using either resected tissue or post-mortem tissues are essential to reveal the underlying histopathological tissue changes in temporal lobe epilepsy. Note that typical anterior temporal lobe resections may be limited to the hippocampus and amygdala and thus may not help clarify histopathological changes throughout the subcortical gray matter.

Conclusion

In this study, we found susceptibility and R_2^* abnormalities in TLE patients compared to healthy controls that affected the hippocampus, amygdala, thalamus, and basal ganglia. Changes observed in our TLE populations provide evidence in support of demyelination in the amygdalae and selective loss of low-myelinated neurons combined with iron redistribution in the hippocampus, predominantly ipsilaterally, indicative of sensitivity to local HS pathology. The increased susceptibility and R_2^* in the thalamus and putamen are concordant with QSM changes related to increased iron content observed in other neurological diseases and seem to reflect disease severity. Further work is required to characterise pathological hippocampal changes that precede hippocampal sclerosis in TLE and that may, in turn, lead to a decrease in hippocampal susceptibility.

Acknowledgments

The authors thank the study participants for their participations, Ms Andrea Hill for contributions to data acquisition and patient selection, Ms Jane de Tisi for help with patient characterisation, Drs Pam Thompson and Sallie Baxendale for collecting and providing neuropsychological data, Prof Matthias Koepp for supporting control data collection, and Dr Carlos Milovic for assistance with FANSI. The authors acknowledge the facilities and scientific and technical assistance of the National Imaging Facility, a National Collaborative Research Infrastructure Strategy (NCRIS) capability, at the Centre for Microscopy, Characterisation, and Analysis, the University of Western Australia.

Funding

Oliver Kiersnowski was supported by EPSRC Doctoral Training Partnership (EP/R513143/1) and EPSRC-funded UCL Centre for Doctoral Training in Intelligent, Integrated Imaging in Healthcare (i4health) (EP/S021930/1). Gavin Winston was supported by the Medical Research Council (MR/M00841X/1). Lorenzo Caciagli was supported by a scholarship from Brain Research UK (ref. 14181). Emma Biondetti was supported by the EPSRC (1489882). John Thornton, John Duncan, and Sjoerd Vos received support from the National Institute for Health Research University College London Hospitals Biomedical Research Centre. Karin Shmueli was supported by European Research Council Consolidator Grant DiSCo MRI SFN 770939.

Competing interests

The authors report no competing interests.

Bibliography

1. Prayson RA. Pathology of Epilepsy. *Practical Surgical Neuropathology: A Diagnostic Approach A Volume in the Pattern Recognition Series*. Published online January 1, 2018:617-632. doi:10.1016/B978-0-323-44941-0.00025-4
2. Özkara Ç, Aronica E. Hippocampal sclerosis. *Handb Clin Neurol*. 2012;108:621-639. doi:10.1016/B978-0-444-52899-5.00019-8
3. Goodkin O, Pemberton HG, Vos SB, et al. Clinical evaluation of automated quantitative MRI reports for assessment of hippocampal sclerosis. *Eur Radiol*. 2021;31(1):34-44. doi:10.1007/s00330-020-07075-2
4. Caciagli L, Bernasconi A, Wiebe S, Koepp MJ, Bernasconi N, Bernhardt BC. A meta-Analysis on progressive atrophy in intractable temporal lobe epilepsy: Time is brain? *Neurology*. 2017;89(5):506-516. doi:10.1212/WNL.0000000000004176
5. Galovic M, Van Dooren VQH, Postma TS, et al. Progressive Cortical Thinning in Patients with Focal Epilepsy. *JAMA Neurol*. 2019;76(10):1230-1239. doi:10.1001/jamaneurol.2019.1708
6. Natsume J, Bernasconi N, Andermann F, Bernasconi A. MRI volumetry of the thalamus in temporal, extratemporal, and idiopathic generalized epilepsy. *Neurology*. Published online 2003. doi:10.1212/01.WNL.0000058764.34968.C2
7. Hatton SN, Huynh KH, Bonilha L, et al. White matter abnormalities across different epilepsy syndromes in adults: An ENIGMA-Epilepsy study. *Brain*. 2020;143(8):2454-2473. doi:10.1093/brain/awaa200
8. He X, Chaitanya G, Asma B, et al. Disrupted basal ganglia-thalamocortical loops in focal to bilateral tonic-clonic seizures. *Brain*. 2020;143(1):175-190. doi:10.1093/brain/awz361
9. Caciagli L, Allen LA, He X, et al. Thalamus and focal to bilateral seizures: A multiscale cognitive imaging study. *Neurology*. 2020;95(17):e2427-e2441. doi:10.1212/WNL.0000000000010645
10. Santyr BG, Goubran M, Lau JC, et al. Investigation of hippocampal substructures in focal temporal lobe epilepsy with and without hippocampal sclerosis at 7T. *Journal of Magnetic Resonance Imaging*. 2017;45(5):1359-1370. doi:10.1002/jmri.25447
11. Winston GP, Vos SB, Caldairou B, et al. Microstructural imaging in temporal lobe epilepsy: Diffusion imaging changes relate to reduced neurite density. *Neuroimage Clin*. 2020;26(February):102231. doi:10.1016/j.nicl.2020.102231
12. Deistung A, Schweser F, Reichenbach JR. Overview of quantitative susceptibility mapping. *NMR Biomed*. 2017;30(4). doi:10.1002/nbm.3569
13. Wang Y, Liu T. Quantitative susceptibility mapping (QSM): Decoding MRI data for a tissue magnetic biomarker. *Magn Reson Med*. 2015;73(1):82-101. doi:10.1002/mrm.25358
14. Shmueli K. Quantitative Susceptibility Mapping. In: *Quantitative Magnetic Resonance Imaging*. 1st ed. Elsevier; 2020.
15. Bilgic B, Langkammer C, Marques JP, Meineke J, Milovic C, Schweser F. QSM reconstruction challenge 2.0: Design and report of results. *Magn Reson Med*. 2021;86(3):1241-1255. doi:10.1002/mrm.28754
16. Langkammer C, Schweser F, Shmueli K, et al. Quantitative susceptibility mapping: Report from the 2016 reconstruction challenge. *Magn Reson Med*. 2018;79(3):1661-1673. doi:10.1002/mrm.26830

17. Eskreis-Winkler S, Zhang Y, Zhang J, et al. The clinical utility of QSM: disease diagnosis, medical management, and surgical planning. *NMR Biomed*. 2017;30(4). doi:10.1002/nbm.3668
18. Wang Y, Spincemaille P, Liu Z, et al. Clinical quantitative susceptibility mapping (QSM): Biometal imaging and its emerging roles in patient care. *Journal of Magnetic Resonance Imaging*. 2017;46(4):951-971. doi:10.1002/jmri.25693
19. Vinayagamani S, Sheelakumari R, Sabarish S, et al. Quantitative Susceptibility Mapping: Technical Considerations and Clinical Applications in Neuroimaging. *Journal of Magnetic Resonance Imaging*. 2021;53(1):23-37. doi:10.1002/jmri.27058
20. Lorio S, Sedlacik J, So PW, et al. Quantitative MRI susceptibility mapping reveals cortical signatures of changes in iron, calcium and zinc in malformations of cortical development in children with drug-resistant epilepsy. *Neuroimage*. 2021;238:118102. doi:10.1016/J.NEUROIMAGE.2021.118102
21. Ebrahimi T, Tafakhori A, Hashemi H, Ali Oghabian M. An interictal measurement of cerebral oxygen extraction fraction in MRI-negative refractory epilepsy using quantitative susceptibility mapping. *Physica Medica*. 2021;85(January):87-97. doi:10.1016/j.ejmp.2021.03.039
22. Adamczyk B, Węgrzyn K, Wilczyński T, Maciarz J, Morawiec N, Adamczyk-Sowa M. The most common lesions detected by neuroimaging as causes of epilepsy. *Medicina (Lithuania)*. 2021;57(3). doi:10.3390/medicina57030294
23. Zimmer TS, David B, Broekaart DWM, et al. Seizure-mediated iron accumulation and dysregulated iron metabolism after status epilepticus and in temporal lobe epilepsy. *Acta Neuropathol*. 2021;142(4):729-759. doi:10.1007/s00401-021-02348-6
24. Cardoso MJ, Modat M, Wolz R, et al. Geodesic Information Flows: Spatially-Variant Graphs and Their Application to Segmentation and Fusion. *IEEE Trans Med Imaging*. 2015;34(9):1976-1988. doi:10.1109/TMI.2015.2418298
25. Prados Carrasco F, Cardoso MJ, Burgos N, Wheeler-Kingshott CAM, Ourselin S. NiftyWeb: web based platform for image processing on the cloud. In: *Scientific Meeting and Exhibition of the International Society for Magnetic Resonance in Medicine -- ISMRM 2016*. ; 2016. https://hal.inria.fr/hal-01827198
26. NiftyWeb. http://niftyweb.cs.ucl.ac.uk/
27. Winston GP, Cardoso MJ, Williams EJ, et al. Automated hippocampal segmentation in patients with epilepsy: Available free online. *Epilepsia*. 2013;54(12):2166-2173. doi:10.1111/epi.12408
28. Modat M, Cash DM, Daga P, Winston GP, Duncan JS, Ourselin S. Global image registration using a symmetric block-matching approach. *Journal of Medical Imaging*. 2014;1(2):024003. doi:10.1117/1.jmi.1.2.024003
29. FANSI Toolbox. https://gitlab.com/cmilovic/FANSI-toolbox
30. Ratcliffe C, Wandschneider B, Baxendale S, Thompson P, Koepp MJ, Caciagli L. Cognitive Function in Genetic Generalized Epilepsies: Insights From Neuropsychology and Neuroimaging. *Front Neurol*. 2020;11(March). doi:10.3389/fneur.2020.00144
31. Liu T, Wisnieff C, Lou M, Chen W, Spincemaille P, Wang Y. Nonlinear formulation of the magnetic field to source relationship for robust quantitative susceptibility mapping. *Magn Reson Med*. 2013;69(2):467-476. doi:10.1002/mrm.24272
32. MEDI Toolbox. http://pre.weill.cornell.edu/mri/pages/qsm.html
33. Schofield MA, Zhu Y. Fast phase unwrapping algorithm for interferometric applications. *Opt Lett*. 2003;28(14):1194. doi:10.1364/ol.28.001194
34. Otsu N. A threshold selection method from gray-level histograms. *IEEE Trans Syst Man Cybern*. 1979;9(1):62-66.

35. Karsa A, Punwani S, Shmueli K. The effect of low resolution and coverage on the accuracy of susceptibility mapping. *Magn Reson Med*. 2019;81(3):1833-1848. doi:10.1002/mrm.27542
36. Kressler B, De Rochefort L, Liu T, Spincemaille P, Jiang Q, Wang Y. Nonlinear regularization for per voxel estimation of magnetic susceptibility distributions from MRI field maps. *IEEE Trans Med Imaging*. 2010;29(2):273-281. doi:10.1109/TMI.2009.2023787
37. Jenkinson M, Beckmann CF, Behrens TEJ, Woolrich MW, Smith SM. FSL. *Neuroimage*. 2012;62(2):782-790. doi:10.1016/j.neuroimage.2011.09.015
38. Kiersnowski OC, Karsa A, Wastling SJ, Thornton JS, Shmueli K. Investigating the effect of oblique image acquisition on the accuracy of QSM and a robust tilt correction method. *Magn Reson Med*. Published online 2022. doi:10.1002/mrm.29550
39. Liu T, Khalidov I, de Rochefort L, et al. A novel background field removal method for MRI using projection onto dipole fields (PDF). *NMR Biomed*. 2011;24(9):1129-1136. doi:10.1002/nbm.1670
40. Schweser F, Robinson SD, de Rochefort L, Li W, Bredies K. An illustrated comparison of processing methods for phase MRI and QSM: removal of background field contributions from sources outside the region of interest. *NMR Biomed*. 2017;30(4). doi:10.1002/nbm.3604
41. Karsa A, Punwani S, Shmueli K. An optimized and highly repeatable MRI acquisition and processing pipeline for quantitative susceptibility mapping in the head-and-neck region. *Magn Reson Med*. 2020;84(6):3206-3222. doi:10.1002/mrm.28377
42. Milovic C, Bilgic B, Zhao B, Acosta-Cabronero J, Tejos C. Fast nonlinear susceptibility inversion with variational regularization. *Magn Reson Med*. 2018;80(2):814-821. doi:10.1002/mrm.27073
43. Milovic C, Bilgic B, Zhao B, Langkammer C, Tejos C, Acosta-Cabronero J. Weak-harmonic regularization for quantitative susceptibility mapping. *Magn Reson Med*. 2019;81(2):1399-1411. doi:10.1002/mrm.27483
44. Murdoch R, Stotesbury H, Hales PW, et al. A Comparison of MRI Quantitative Susceptibility Mapping and TRUST-Based Measures of Brain Venous Oxygen Saturation in Sickle Cell Anaemia. *Front Physiol*. 2022;13. doi:10.3389/fphys.2022.913443
45. Murdoch R, Stotesbury H, Kawadler JM, Saunders DE, Kirkham FJ, Shmueli K. *Quantitative Susceptibility Mapping (QSM) and R2* of Silent Cerebral Infarcts in Sickle Cell Anemia*.
46. Hansen PC. The L-curve and its use in the numerical treatment of inverse problems. 2:1-24.
47. Gudbjartsson H, Patz S. The rician distribution of noisy mri data. *Magn Reson Med*. 1995;34(6):910-914. doi:10.1002/mrm.1910340618
48. Bilgic B, Chatnuntawech I, Langkammer C, Setsompop K. *Sparse Methods for Quantitative Susceptibility Mapping*.; 2015. doi:10.1117/12.2188535
49. Milovic C, Prieto C, Bilgic B, et al. Comparison of parameter optimization methods for quantitative susceptibility mapping. *Magn Reson Med*. 2021;85(1):480-494. doi:10.1002/mrm.28435
50. Zhang Y, Wei H, Cronin MJ, He N, Yan F, Liu C. Longitudinal atlas for normative human brain development and aging over the lifespan using quantitative susceptibility mapping. *Neuroimage*. 2018;171:176-189. doi:10.1016/j.neuroimage.2018.01.008
51. Li W, Wu B, Batrachenko A, et al. Differential developmental trajectories of magnetic susceptibility in human brain gray and white matter over the lifespan. *Hum Brain Mapp*. 2014;35(6):2698-2713. doi:10.1002/hbm.22360

52. Acosta-Cabronero J, Betts MJ, Cardenas-Blanco A, Yang S, Nestor PJ. In vivo MRI mapping of brain iron deposition across the adult lifespan. *Journal of Neuroscience*. 2016;36(2):364-374. doi:10.1523/JNEUROSCI.1907-15.2016
53. O'Muircheartaigh J, Vollmar C, Barker GJ, et al. Abnormal thalamocortical structural and functional connectivity in juvenile myoclonic epilepsy. *Brain*. 2012;135(12):3635-3644. doi:10.1093/brain/aws296
54. Xiao F, Caciagli L, Wandschneider B, et al. Effects of carbamazepine and lamotrigine on functional magnetic resonance imaging cognitive networks. *Epilepsia*. 2018;59(7):1362-1371. doi:10.1111/epi.14448
55. Viñas-Guasch N, Wu YJ. The role of the putamen in language: a meta-analytic connectivity modeling study. *Brain Struct Funct*. 2017;222(9):3991-4004. doi:10.1007/s00429-017-1450-y
56. Duyn JH, Schenck J. Contributions to magnetic susceptibility of brain tissue. *NMR Biomed*. 2017;30(4). doi:10.1002/nbm.3546
57. Thom M. Review: Hippocampal sclerosis in epilepsy: A neuropathology review. *Neuropathol Appl Neurobiol*. 2014;40(5):520-543. doi:10.1111/nan.12150
58. DeKraker J, Ferko KM, Lau JC, Köhler S, Khan AR. Unfolding the hippocampus: An intrinsic coordinate system for subfield segmentations and quantitative mapping. *Neuroimage*. 2018;167(June 2017):408-418. doi:10.1016/j.neuroimage.2017.11.054
59. Krogsrud SK, Tamnes CK, Fjell AM, et al. Development of hippocampal subfield volumes from 4 to 22 years. *Hum Brain Mapp*. 2014;35(11):5646-5657. doi:10.1002/hbm.22576
60. Schweser F, Hagemeier J, Dwyer MG, et al. Decreasing brain iron in multiple sclerosis: The difference between concentration and content in iron MRI. *Hum Brain Mapp*. 2021;42(5):1463-1474. doi:10.1002/hbm.25306
61. Van Bergen JMG, Hua J, Unschuld PG, et al. Quantitative susceptibility mapping suggests altered brain iron in premanifest Huntington disease. *American Journal of Neuroradiology*. 2016;37(5):789-796. doi:10.3174/ajnr.A4617
62. Harrison DM, Li X, Liu H, et al. Lesion heterogeneity on high-field susceptibility MRI Is associated with multiple sclerosis severity. *American Journal of Neuroradiology*. 2016;37(8):1447-1453. doi:10.3174/ajnr.A4726
63. Birkl C, Birkl-Toeglhofer AM, Kames C, et al. The influence of iron oxidation state on quantitative MRI parameters in post mortem human brain. *Neuroimage*. 2020;220. doi:10.1016/j.neuroimage.2020.117080
64. Gleissner U, Elger CE. The hippocampal contribution to verbal fluency in patients with temporal lobe epilepsy. *Cortex*. 2001;37(1):55-63. doi:10.1016/S0010-9452(08)70557-4
65. Kullmann DM. What's wrong with the amygdala in temporal lobe epilepsy? *Brain*. 2011;134(10):2800-2801. doi:10.1093/brain/awr246
66. Cendes F, Andermann F, Gloor P, et al. MRI volumetric measurement of amygdala and hippocampus in temporal lobe epilepsy. *Neurology*. 1993;43(4):719 LP - 719. doi:10.1212/WNL.43.4.719
67. Kälviäinen R, Salmenperä T, Partanen K, Vainio P, Riekkinen P, Pitkänen A. MRI volumetry and T2 relaxometry of the amygdala in newly diagnosed and chronic temporal lobe epilepsy. *Epilepsy Res*. 1997;28(1):39-50. doi:10.1016/S0920-1211(97)00029-6
68. Nakayama Y, Masuda H, Shirozu H, et al. Features of amygdala in patients with mesial temporal lobe epilepsy and hippocampal sclerosis: An MRI volumetric and histopathological study. *Epilepsy Res*. 2017;135(May):50-55. doi:10.1016/j.eplepsyres.2017.05.010

69. Schramm J. Temporal lobe epilepsy surgery and the quest for optimal extent of resection: A review. *Epilepsia*. 2008;49(8):1296-1307. doi:10.1111/j.1528-1167.2008.01604.x
70. Keller SS, Ahrens T, Mohammadi S, et al. Voxel-based statistical analysis of fractional anisotropy and mean diffusivity in patients with unilateral temporal lobe epilepsy of unknown cause. *Journal of Neuroimaging*. 2013;23(3):352-359. doi:10.1111/j.1552-6569.2011.00673.x
71. Allen LA, Harper RM, Kumar R, et al. Dysfunctional brain networking among autonomic regulatory structures in temporal lobe epilepsy patients at High Risk of sudden unexpected death in epilepsy. *Front Neurol*. 2017;8(OCT):1-13. doi:10.3389/fneur.2017.00544
72. Keller SS, O'Muircheartaigh J, Traynor C, Towgood K, Barker GJ, Richardson MP. Thalamotemporal impairment in temporal lobe epilepsy: A combined MRI analysis of structure, integrity, and connectivity. *Epilepsia*. 2014;55(2):306-315. doi:10.1111/epi.12520
73. Li J, Li Y, Gutierrez L, et al. Imaging the Centromedian Thalamic Nucleus Using Quantitative Susceptibility Mapping. *Front Hum Neurosci*. 2020;13(January):1-7. doi:10.3389/fnhum.2019.00447
74. Xu X, Wang Q, Zhang M. Age, gender, and hemispheric differences in iron deposition in the human brain: An in vivo MRI study. *Neuroimage*. 2008;40(1):35-42. doi:10.1016/j.neuroimage.2007.11.017
75. Pulsipher DT, Seidenberg M, Morton JJ, Geary E, Parrish J, Hermann B. MRI volume loss of subcortical structures in unilateral temporal lobe epilepsy. *Epilepsy and Behavior*. 2007;11(3):442-449. doi:10.1016/j.yebeh.2007.08.007
76. Dabbs K, Becker T, Jones J, Rutecki P, Seidenberg M, Hermann B. Brain structure and aging in chronic temporal lobe epilepsy. *Epilepsia*. 2012;53(6):1033-1043. doi:10.1111/j.1528-1167.2012.03447.x
77. Park KM, Lee BI, Shin KJ, et al. Pivotal role of subcortical structures as a network hub in focal epilepsy: Evidence from graph theoretical analysis based on diffusion-tensor imaging. *Journal of Clinical Neurology (Korea)*. 2019;15(1):68-76. doi:10.3988/jcn.2019.15.1.68
78. Hermann BP, Seidenberg M, Schoenfeld J, Davies K. Neuropsychological Characteristics of the Syndrome of Mesial Temporal Lobe Epilepsy. *Arch Neurol*. 1997;54(4):369-376. doi:10.1001/archneur.1997.00550160019010
79. Acosta-Cabronero J, Williams GB, Cardenas-Blanco A, Arnold RJ, Lupson V, Nestor PJ. In vivo quantitative susceptibility mapping (QSM) in Alzheimer's disease. *PLoS One*. 2013;8(11). doi:10.1371/journal.pone.0081093
80. Thomas GEC, Leyland LA, Schrag AE, Lees AJ, Acosta-Cabronero J, Weil RS. Brain iron deposition is linked with cognitive severity in Parkinson's disease. *J Neurol Neurosurg Psychiatry*. 2020;91(4):418-425. doi:10.1136/jnnp-2019-322042
81. Damulina A, Pirpamer L, Soellradl M, et al. Cross-sectional and longitudinal assessment of brain iron level in Alzheimer disease using 3-T MRI. *Radiology*. 2020;296(3):619-626. doi:10.1148/radiol.2020192541
82. Cole AJ. Is epilepsy a progressive disease? The neurobiological consequences of epilepsy. *Epilepsia*. 2000;41(6 SUPPL. 2). doi:10.1111/j.1528-1157.2000.tb01520.x
83. Sutula TP, Hagen J, Pitkänen A. Do epileptic seizures damage the brain? *Curr Opin Neurol*. 2003;16(2):189-195. doi:10.1097/01.wco.0000063770.15877.bc
84. Rossini L, Garbelli R, Gnatkovsky V, et al. Seizure activity per se does not induce tissue damage markers in human neocortical focal epilepsy. *Ann Neurol*. 2017;82(3):331-341. doi:10.1002/ana.25005

85. Schweser F. Recommended implementation of quantitative susceptibility mapping for clinical research in the brain: Consensus of the QSM community [Presentation]. *QMR Lucca: Joint Workshop on MR phase, magnetic susceptibility and electrical properties mapping*. Published online October 18, 2022.
86. Treit S, Naji N, Seres P, et al. R2* and quantitative susceptibility mapping in deep gray matter of 498 healthy controls from 5 to 90 years. *Hum Brain Mapp*. 2021;42(14):4597-4610. doi:10.1002/hbm.25569

Figure Captions

Figure 1: Images from a representative subject: T1-weighted image, gradient echo magnitude image, R2* map and Susceptibility map. a) T1-weighted image with ROIs superimposed (putamen – green, globus pallidus – pink, caudate nucleus – blue, thalamus – brown, amygdala – red, hippocampus - yellow) b) last echo gradient echo magnitude image c) R_2^* map d) susceptibility (χ) map calculated with the optimised weak harmonic QSM method.

Figure 2: Comparison of susceptibility calculation techniques. Comparison of the three susceptibility (χ) calculation methods in a representative RTLE subject: iterative Tikhonov regularisation (left), non-linear total variation (middle) and weak harmonic QSM (right). Difference images are relative to the iterative Tikhonov regularisation susceptibility map. Iterative Tikhonov suffers from high noise and residual background fields. WH-QSM performs the best, removing both noise and residual background fields. This is most evident in the cerebellum (red arrows) and the top of the brain (blue arrows). Axial and sagittal slice positions are indicated by the green dashed lines.

Figure 3: Comparison of standard deviation across susceptibility calculation techniques. The average standard deviation of susceptibility values in each ROI, over all participants regardless of disease state, was compared across the three QSM methods: iterative Tikhonov regularisation (iterTik), non-linear total variation (nlTV) and weak harmonic QSM (WH-QSM). WH-QSM consistently had the lowest standard deviation for all ROIs. An outlier (STD > 0.25) in the left and right amygdala in the non-linear TV group has been omitted to facilitate comparison. * indicates P<0.05, ** indicates P<0.01, *** indicates P<0.001.

Figure 4: Significant ROI mean susceptibility differences between TLE and healthy control groups. Boxplots showing comparison of average susceptibility (χ) across the three groups. * indicates P<0.05, *** indicates P < 0.001. Abbreviations: HC: healthy controls; LTLE: left temporal lobe epilepsy; RTLE: right temporal lobe epilepsy

Figure 5: Significant ROI mean R_2^* differences between TLE and healthy control groups. Significant R_2^* group changes in six ROIs are shown. Both pathological hippocampi in their respective TLE group were found to have significantly reduced R_2^* values. * indicates P<0.05, ** indicates P<0.01, *** indicates P<0.001.

Figure 6: Susceptibility and R_2^* versus age of TLE onset. Scatterplots showing caudate R_2^* and hippocampal and putamen susceptibility (χ) versus age of TLE onset. Dots indicate people with left temporal lobe epilepsy (TLE); crosses indicate people with right TLE. Dashed (left TLE) and dotted (right TLE) lines indicate plots of linear correlation for regions with significant correlations. These lines are shown only as a visual aid as significance testing was performed using Spearman rank correlation.

Figure 7: Susceptibility and R_2^* versus log-transformed frequency of FBTCS. Scatterplots showing thalamic and putamen susceptibility (χ) and R_2^* in the globi pallidi against the frequency of focal to bilateral tonic-clonic seizures (FBTCS), log-transformed to ensure normality. Dots indicate people with left temporal lobe epilepsy (TLE); crosses indicate people with right TLE; the black line indicates the linear fit of significantly correlated factors.